# DoF Analysis for Multipath-Assisted Imaging: Single Frequency Illumination

Nishant Mehrotra and Ashutosh Sabharwal
Department of Electrical and Computer Engineering
Rice University
{nm30, ashu}@rice.edu

Abstract—Multipath-assisted imaging algorithms have been shown to achieve super-resolution by incorporating multipath information into the imaging pipeline. In this paper, we derive the imaging degrees of freedom for multipath-assisted imaging systems to quantify the amount of super-resolution possible.

#### I. Introduction

Super-resolution imaging techniques attempt to break conventional diffraction limits by extracting more information from the spectra of the measured data than that usually available. For conventional LOS imaging models that assume the imaging targets to be embedded in free space, it has been argued in [1]–[3] that super-resolution requires an exponential increase in resources to extract data beyond the well-known degrees of freedom limit [4], [5].

However, for urban radar imaging setups, it has been shown experimentally and numerically in [6]–[11] that scattering (multipath) results in better imaging resolution as compared to that possible with conventional LOS models. We term such imaging algorithms as *multipath-assisted* imaging algorithms.

In this paper, we theoretically establish multipath-assisted super-resolution via an imaging degrees of freedom analysis.

**Related literature:** Our system model is most closely related with that of [12], [13], where the spatial degrees of freedom for wireless networks in the presence of external scatterers is studied. For a *closed* cut-set completely surrounding the transmitter volume, in [13] it is shown that no superresolution is possible in the limit of large radiating systems.

However, the model considered in [12], [13] corresponds to an aperture subtending the angle  $\Omega_{ap}=2\pi$  at the center of the transmitter volume, which is unrepresentative of practical imaging apertures (where  $\Omega_{ap}<2\pi$ ).

The  $\Omega_{ap}$  <  $2\pi$  case has previously been considered for LOS imaging in [14] and with multipath in [15]. However, in [15] only heuristics based DoF formulae are presented; in this paper we theoretically show the increase in DoF by extending the LOS DoF framework of [4], [5], [14] to our system model with multipath. Our results explain the numerical observations of [6]–[11], [15] for a single frequency illumination model.

**Contributions:** We present a degrees of freedom analysis for multipath-assisted imaging algorithms. Our main result consists of upper and lower bounds on the imaging DoF for apertures with angular extent  $\Omega_{ap} < 2\pi$ . We also establish that with multipath, the singular values of the imaging channel exhibit a heavy tail decay beyond the LOS DoF. Our analysis 978-1-7281-6432-8/20/\$31.00 ©2020 IEEE 1456

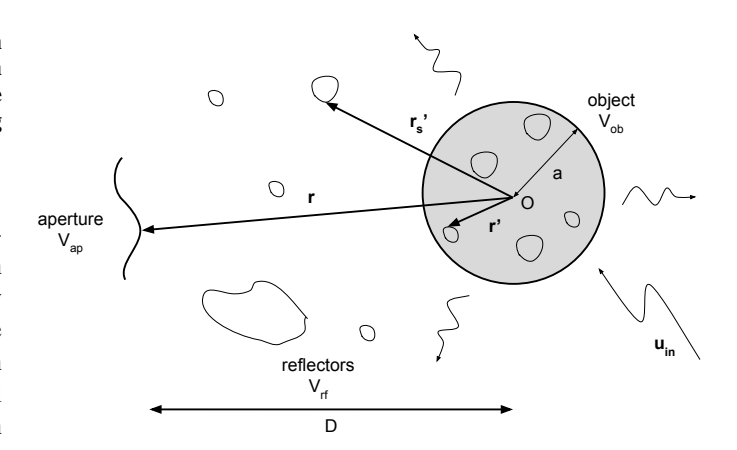


Fig. 1. System model for 2D imaging.

remains consistent with [13] when  $\Omega_{ap} = 2\pi$ ; no DoF increase over LOS is predicted in this scenario.

**Outline:** The paper is organized as follows. We present the multipath-assisted imaging system model in Section II. In Section III, we formulate the degrees of freedom analysis problem. We then derive our main results in Section IV and present numerical evaluation of our theoretical results in Section V. In Section VI we conclude the paper with discussions and some directions for future work.

#### II. SYSTEM MODEL

Consider a spherical volume  $V_{ob} \subset \mathbb{R}^N$  of radius a located at the origin such that the imaging targets are wholly enclosed within it. Reflectors external to  $V_{ob}$  are located in  $V_{rf} \subset \mathbb{R}^N$ . The imaging aperture  $V_{ap} \subset \mathbb{R}^{N-1}$  is located at a minimum distance D from the origin. Figure 1 depicts the system model under consideration for 2D imaging (N=2).

As we are only interested in imaging the targets inside  $V_{ob}$ , we subtract out the direct backscatter from  $V_{rf}$  from the total field. The Fourier transform of the resulting field is

$$\mathbf{E}(s) = \int_{V_{ab}} \hat{\mathbf{G}}(s, \mathbf{r}') \cdot \mathbf{I}(\mathbf{r}') d\mathbf{r}', \tag{1}$$

where  $\mathbf{I}(\mathbf{r}')$ ,  $\mathbf{r}' \in V_{ob}$  denotes the current densities induced in  $V_{ob}$  due to the illuminating field  $\mathbf{u}_{in}$ .  $\hat{\mathbf{G}}(\cdot, \cdot)$  is the combined multipath Green's function,

$$\hat{\mathbf{G}}(s, \mathbf{r}') = \mathbf{G}(s, \mathbf{r}') + \tilde{\mathbf{G}}(s, \mathbf{r}'),$$

$$\mathbf{G}(s, \mathbf{r}') = \mathbf{G}(s, \mathbf{r}') + \tilde{\mathbf{G}}(s, \mathbf{r}')$$

where  $G(\cdot, \cdot)$  denotes the LOS Green's function and  $G(\cdot, \cdot)$  denotes the NLOS Green's function,

$$\tilde{\mathbf{G}}(s, \mathbf{r}') = \int_{V_{rf}} h(\mathbf{r}'_s) \mathbf{G}(s, \mathbf{r}'_s) \mathbf{G}(\mathbf{r}'_s, \mathbf{r}') d\mathbf{r}'_s.$$
(3)

In the equation above,  $h(\cdot)$  denotes the reflectivities of the reflectors in  $V_{rf}$  and  $s=s(\mathbf{r})$ ,  $\mathbf{r}\in V_{ap}$  is a coordinate system defined over  $V_{ap}$  such that s is normalized to D. Let  $\mathcal{E}_m$  be the space of all measured fields for our multipath system model.

#### III. PROBLEM FORMULATION

The goal of degrees of freedom analysis is to identify the dimensions of the smallest possible subspace that can approximate the *space* of the measured fields  $\mathcal{E}_m$  up to an arbitrarily small precision. To characterize the space of all measured fields, we consider the signals flowing through the cut-set shown in Figure 2 that separates  $V_{ob}$  from  $V_{rf}$  and  $V_{ap}$ .

# A. Space of Measured Fields

To characterize the space of all measured fields, we consider the *support sets* of the signals flowing through the cut-set in the spatial and the spatial frequency (wavenumber) domains.

The spatial support is determined by the angular extent (as seen from the origin) of the physical aperture,  $\Omega_{ap}$ , and that of the reflector volume,  $\Omega_{ap}^m$ . The wavenumber support is governed by the spatial bandwidth, whose value we evaluate in Section IV-A. We also derive conditions under which the spatial bandwidth is well-defined in Section IV-B.

## B. Degrees of Freedom Analysis

We use the following definition for the degrees of freedom: Definition 1: The degrees of freedom (DoF)  $N_{\epsilon}(A)$  required to approximate a set A up to an accuracy of  $\epsilon$  is defined as

$$N_{\epsilon}(\mathcal{A}) = \min \{ N : d_N(\mathcal{A}) \le \epsilon \},$$

where  $d_N\left(\mathcal{A}\right)$  is the Kolmogorov N-width [16], defined as  $Definition\ 2$ : The Kolmogorov N-width  $d_N\left(\mathcal{A}\right)$  of a space  $\mathcal{A}$  that is to be approximated by N-dimensional subspaces  $\mathcal{X}_N$  of a normed linear space  $\mathcal{X}$  is

$$d_{N}(\mathcal{A}) = \inf_{\mathcal{X}_{N} \subseteq \mathcal{X}} \sup_{f \in \mathcal{A}} \inf_{g \in \mathcal{X}_{N}} \|f - g\|.$$

In Section IV-C we derive upper and lower bounds on the DoF for our system model when  $\mathcal{A} = \mathcal{E}_m$ ,  $\mathcal{X}$  is the optimal PSWF basis and the choice of the norm corresponds to the  $\mathcal{L}_2$  norm over the measurable set on which the PSWF basis is maximally concentrated.

#### IV. MAIN RESULTS

# A. Spatial Bandwidth W

We first present a lemma on the spatial bandwidth for the sum of two spatially bandlimited fields before deriving the spatial bandwidth W for our system model in Corollary 1.

*Lemma 1:* Given two fields  $\mathbf{E}_1(s)$  and  $\mathbf{E}_2(s)$  with spatial bandwidths  $W_1$  and  $W_2$  respectively, the spatial bandwidth W for their sum  $\mathbf{E}_1(s) + \mathbf{E}_2(s)$  is given by

$$W = \max\{W_1, W_2\}.$$

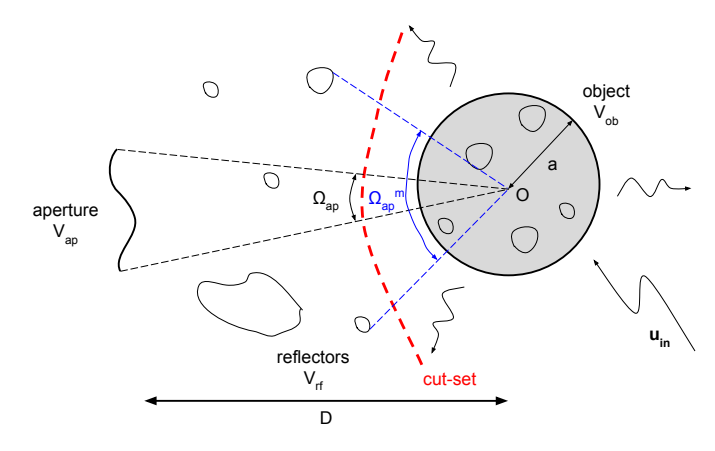


Fig. 2. Cut-set for degrees of freedom analysis.

*Proof:* Define  $G_1(\cdot,\cdot)$  and  $G_2(\cdot,\cdot)$  such that

$$\mathbf{E}_{1}(s) = \int_{V} \mathbf{G}_{1}(s, \mathbf{r}') \cdot \mathbf{I}(\mathbf{r}') \, d\mathbf{r}', \tag{4}$$

$$\mathbf{E}_{2}(s) = \int_{V} \mathbf{G}_{2}(s, \mathbf{r}') \cdot \mathbf{I}(\mathbf{r}') \, d\mathbf{r}', \tag{5}$$

and let  $\mathbf{E}(s) = \mathbf{E}_1(s) + \mathbf{E}_2(s)$ ,  $\mathbf{G}(s, \mathbf{r}') = \mathbf{G}_1(s, \mathbf{r}') + \mathbf{G}_2(s, \mathbf{r}')$  and denote the set of all possible fields  $\mathbf{E}(s)$  by  $\mathcal{E}$ . To approximate  $\mathcal{E}$  by  $\mathcal{B}_w$ , we pass  $\mathbf{E}(s)$  through an ideal low-pass filter with wavenumber support w to obtain [4]

$$\mathbf{E}_{w}(s) = \frac{1}{\pi} \frac{\sin(ws)}{s} * \mathbf{E}(s) = \int_{V} \mathbf{G}_{w}(s, \mathbf{r}') \cdot \mathbf{I}(\mathbf{r}') d\mathbf{r}', (6)$$

where  $\mathbf{G}_w\left(s,\mathbf{r}'\right) = \frac{1}{\pi} \frac{\sin(ws)}{s} * \mathbf{G}\left(s,\mathbf{r}'\right)$  is the filtered Green's function and \* denotes convolution in the s domain.

The spatial bandwidth corresponds to the value W such that deviation  $D_{\mathcal{B}_w}\left(\mathcal{E}\right)$  between the sets  $\mathcal{E}$  and  $\mathcal{B}_w$  vanishes for all  $w \geq W$ . Here,  $D_{\mathcal{B}_w}\left(\mathcal{E}\right)$  is given by the  $\mathcal{L}_2\left(-\infty,\infty\right)$  norm of the error  $\Delta\mathbf{E}\left(s\right) = \mathbf{E}\left(s\right) - \mathbf{E}_w\left(s\right)$ ,

$$D_{\mathcal{B}_{w}}\left(\mathcal{E}\right) = \left\|\Delta\mathbf{E}\left(s\right)\right\|_{2}^{2} = \int_{-\infty}^{\infty} \left|\Delta\mathbf{E}\left(s\right)\right|^{2} \mathrm{d}s,\tag{7}$$

where  $\Delta \mathbf{E}(s) = \int_{V} \Delta \mathbf{G}(s, \mathbf{r}') \cdot \mathbf{I}(\mathbf{r}') d\mathbf{r}'$  and  $\Delta \mathbf{G}(s, \mathbf{r}') = \mathbf{G}(s, \mathbf{r}') - \mathbf{G}_{w}(s, \mathbf{r}') = \Delta \mathbf{G}_{1}(s, \mathbf{r}') + \Delta \mathbf{G}_{2}(s, \mathbf{r}')$ .

To minimize  $D_{\mathcal{B}_w}(\mathcal{E})$ , we minimize an upper bound to it obtained via Young's inequality [4]

$$\|\Delta \mathbf{E}(s)\|_{2}^{2} \leq \sup_{\mathbf{r}' \in V} \left( \|\Delta \mathbf{G}(s, \mathbf{r}')\|_{2}^{2} \right) \cdot \|\mathbf{I}(\mathbf{r}')\|_{1}^{2}.$$
 (8)

For finite  $\|\mathbf{I}(\mathbf{r}')\|_1^2$ , the RHS above may be minimized by choosing W such that the term  $\sup_{\mathbf{r}' \in V} \left( \|\Delta \mathbf{G}(s, \mathbf{r}')\|_2^2 \right)$  vanishes for all  $w \geq W$ . To relate W with  $W_1$  and  $W_2$ , we further upper bound the RHS by noting that

$$\|\Delta \mathbf{G}(s, \mathbf{r}')\|_{2}^{2} \le 2 \|\Delta \mathbf{G}_{1}(s, \mathbf{r}')\|_{2}^{2} + 2 \|\Delta \mathbf{G}_{2}(s, \mathbf{r}')\|_{2}^{2},$$
 (9)

via the triangle inequality and Jensen's inequality. Therefore, it suffices to choose  $W = \max\{W_1, W_2\}$  to ensure that both terms on the RHS of (9) vanish for all  $w \ge W$ .

Corollary 1: To apply the results of Lemma 1 to our system model in Section II, we substitute  $\mathbf{G}_1(s,\mathbf{r}')=\mathbf{G}(s,\mathbf{r}')$ ,  $\mathbf{G}_2(s,\mathbf{r}')=\tilde{\mathbf{G}}(s,\mathbf{r}')$ ,  $V=V_{ob}$  and  $\mathcal{E}=\mathcal{E}_m$ . From the main results in [4] and [13], we know that  $W_1=W_2=k_0a$ , where  $k_0=\frac{2\pi}{\lambda}$  is the wavenumber given the illumination wavelength  $\lambda$ . Therefore, from Lemma 1, the optimal spatial bandwidth for our system model is  $W=\max\{W_1,W_2\}=k_0a$ .

### B. Well-Definedness of W

The spatial bandwidth derived in Corollary 1 is only well-defined if the upper bound to the deviation  $D_{\mathcal{B}_w}\left(\mathcal{E}_m\right)$  can be made as small as desired (for all  $w \geq W$ ) independent of the value of the current densities induced on the targets and reflectors. This is only possible if  $\|\mathbf{I}(\mathbf{r}')\|_1$  is finite to prevent any super-gain effects from occurring.

Lemma 2: The spatial bandwidth W is well-defined when

$$\sup_{\mathbf{r}'' \in V_{ob}} \left( \left\| f\left(\mathbf{r}'\right) \tilde{\mathbf{G}}\left(\mathbf{r}', \mathbf{r}''\right) \right\|_{1} \right) < 1.$$

*Proof:* From the system model, we have

$$\mathbf{I}(\mathbf{r}') = \mathbf{I}_{in}(\mathbf{r}') + f(\mathbf{r}') \int_{V_{rf}} \mathbf{G}(\mathbf{r}', \mathbf{r}'_s) \cdot \mathbf{I}(\mathbf{r}'_s) d\mathbf{r}'_s, \quad (10)$$

$$\mathbf{I}(\mathbf{r}'_s) = \mathbf{I}_{in}(\mathbf{r}'_s) + h(\mathbf{r}'_s) \int_{V_{-1}} \mathbf{G}(\mathbf{r}'_s, \mathbf{r}') \cdot \mathbf{I}(\mathbf{r}') d\mathbf{r}', \quad (11)$$

where  $f(\cdot)$  and  $h(\cdot)$  are the reflectivities of the targets and reflectors respectively. On substituting (11) in (10), rearranging, and applying the triangle and Young's inequalities, we obtain

$$\|\mathbf{I}(\mathbf{r}')\|_{1} \leq \|\mathbf{I}(\mathbf{r}')\|_{1} \cdot \sup_{\mathbf{r}'' \in V_{ob}} \left( \left\| f(\mathbf{r}') \, \tilde{\mathbf{G}}(\mathbf{r}', \mathbf{r}'') \right\|_{1} \right) + \left\| \mathbf{I}_{in}(\mathbf{r}') + f(\mathbf{r}') \int_{V_{rf}} \mathbf{G}(\mathbf{r}', \mathbf{r}'_{s}) \cdot \mathbf{I}_{in}(\mathbf{r}'_{s}) \, d\mathbf{r}'_{s} \right\|_{1}, \quad (12)$$

where  $\tilde{\mathbf{G}}(\cdot,\cdot)$  is the NLOS Green's function defined in (3). From the impossibility of super-gain i.e.  $\|\mathbf{I}(\mathbf{r}')\|_1 < \infty$  and (12), the desired condition is readily obtained.

# C. Degrees of Freedom Analysis

Given the spatial bandwidth is well-defined, the degrees of freedom required to approximate  $\mathcal{E}_m$  up to an accuracy of  $\epsilon$  can be evaluated via Definition 1. As  $D_{\mathcal{B}_w}\left(\mathcal{E}_m\right) \leq \delta$  for arbitrarily small  $\delta > 0$  for all  $w \geq W$ ; we may approximate  $\mathcal{E}_m$  by the space of *unit energy, bandlimited signals*,  $\mathcal{B}_W$ , where the bandlimitation is to the spatial bandwidth W [4], [5], [17].

As per Definitions 1 and 2, it is necessary to choose an appropriate basis  $\mathcal X$  and norm  $\|\cdot\|$  for the degrees of freedom to be defined. To do so, we characterize the spatial support in terms of the angular extents  $\Omega_{ap}$  and  $\Omega^m_{ap}$  introduced in Section III-A by defining sets  $S_l$  and  $S_i$ ,

$$S_l = \left\{ s : s = s(\mathbf{r}), \mathbf{r} \in V_{ap} \right\},\tag{13}$$

$$S_i = \{s' : s' = s'(\mathbf{r}'_s), \mathbf{r}'_s \in V_{rf,ap} \subseteq V_{rf}\}, \tag{14}$$

where  $V_{rf,ap}$  is a subset of  $V_{rf}$  that includes all reflector—choosing  $\mathcal{X}$  as the PSWF basis maximally collocations that result in scattering towards  $V_{ap}$ . For instance, and using the  $\mathcal{L}_2(S_u)$  norm in Definition 1.

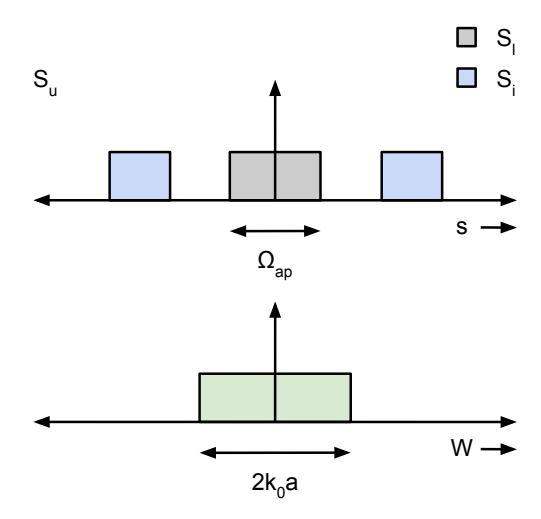


Fig. 3. Spatial and wavenumber support sets for 2D imaging (with  $\kappa=3$ ).

when the reflectors are diffuse,  $V_{rf,ap} = V_{rf}$ . However, for specular reflectors,  $V_{rf,ap} \subset V_{rf}$  only includes the reflector locations that are oriented appropriately to scatter incoming waves towards  $V_{ap}$ . Note that in the definitions above, s (resp. s') is a normalized coordinate system defined over  $V_{ap}$  (resp.  $V_{rf,ap}$ ) such that every element of  $S_l$  (resp.  $S_i$ ) corresponds to the azimuth angle of the ray joining the origin and  $\mathbf{r}$  (resp.  $\mathbf{r}'_s$ ). Thus, for the Lebesgue measure  $m(\cdot)$ , we have  $m(S_l) \leq \Omega_{ap}$  (resp.  $m(S_i) \leq \Omega_{ap}^m$ ) with equality only when the physical aperture is continuous (resp. when the reflectors are diffuse i.e.  $V_{rf,ap} = V_{rf}$  and when  $V_{rf}$  is densely populated).

Having defined  $S_l$  and  $S_i$ , we define the *spatial support set*  $S_u = S_l \cup S_i$  as the union of the non-overlapping elements of  $S_l$  and  $S_i$ . Let the set  $S_u$  consist of  $\kappa \geq 1$  disjoint intervals. In Figure 3 we show a generic example of the support sets for 2D imaging with a continuous physical aperture.

Theorem 1: The degrees of freedom  $N_{\epsilon}(\mathcal{E}_m)$  is upper and lower bounded as  $N_l \leq N_{\epsilon}(\mathcal{E}_m) \leq N_u$ ,

$$\begin{split} N_{l} &= N_{0,l} + \frac{1}{\pi^{2}} \ln \left( \frac{1 - \epsilon^{2}}{\epsilon^{2}} \right) \ln \left( \frac{\pi N_{0,l}}{2} \right) + O\left( \ln \left( N_{0,l} \right) \right), \\ N_{u} &= N_{0,u} + \frac{\kappa}{\pi^{2}} \ln \left( \frac{1 - \epsilon^{2}}{\epsilon^{2}} \right) \ln \left( \frac{\pi N_{0,u}}{2} \right) + O\left( \ln \left( N_{0,u} \right) \right), \end{split}$$

where 
$$N_{0,l}=\frac{Wm(S_l)}{\pi},~N_{0,u}=\frac{Wm(S_u)}{\pi}$$
 and  $W=\frac{2\pi a}{\lambda}.$  Proof: As multipath results in further attenuation in

*Proof:* As multipath results in further attenuation in NLOS compared to LOS due to the reflectivity  $h(\mathbf{r}'_s)$  of the reflectors, the DoF  $N_{\epsilon}(\mathcal{E}_m)$  is highly dependent on the reflectivity of the reflectors. Therefore, we only attempt to bound the DoF from above and below. Our lower bound corresponds to choosing  $h(\mathbf{r}'_s) = 0$  everywhere in  $V_{rf}$ ; this is equivalent to the LOS DoF i.e. choosing  $\mathcal{X}$  as the PSWF basis maximally concentrated on  $S_l$  and using the  $\mathcal{L}_2(S_l)$  norm in Definition 1. Similarly, our upper bound corresponds to choosing  $h(\mathbf{r}'_s) = 1$  everywhere in  $V_{rf}$ ; this is equivalent to choosing  $\mathcal{X}$  as the PSWF basis maximally concentrated on  $S_u$  and using the  $\mathcal{L}_2(S_u)$  norm in Definition 1.

Note that given S and the  $\mathcal{L}_2(S)$  norm, the Kolmogorov N-width  $d_N(\mathcal{B}_W)$  is [4], [5], [16], [18], [19]

$$d_N\left(\mathcal{B}_W\right) = \sqrt{\lambda_N},\tag{15}$$

i.e. the Nth eigenvalue of the PSWF integral equation,

$$\int_{S} \frac{\sin(W(s-s''))}{\pi(s-s'')} \psi_{N}(s'') ds'' = \lambda_{N} \psi_{N}(s), \ s \in S.$$
 (16)

 $\psi_N(s)$  in (16) is the Nth bandlimited PSWF basis function,  $\psi_N(s) \in \mathcal{B}_W$ , such that  $\int_{\mathbb{R}} \psi_N(s) \psi_M(s) \mathrm{d}s = \delta_{N,M}$  and  $\int_S \psi_N(s) \psi_M(s) ds = \delta_{N,M} \lambda_N$  for  $N \neq M$  and the Kronecker delta function  $\delta_{N,M}$ . Thus, when  $\mathcal{X}$  is the PSWF basis maximally concentrated on S and the  $\mathcal{L}_2(S)$  norm is used, from Definition 1 and the results of [16], [18]-[20] we have

$$N_{\epsilon}\left(\mathcal{B}_{W}\right) = \frac{Wm(S)}{\pi} + \Delta,\tag{17}$$

where the additional term  $\Delta$  is logarithmic in  $N_0 = \frac{Wm(S)}{\tau}$ and is weakly dependent on  $\epsilon$ ,

$$\Delta = \frac{\kappa'}{\pi^2} \ln \left( \frac{1 - \epsilon^2}{\epsilon^2} \right) \ln \left( \frac{\pi N_0}{2} \right) + O\left( \ln \left( N_0 \right) \right), \quad (18)$$

for  $\kappa'$  disjoint intervals in S. Thus, our result follows on choosing  $S = S_l$ ,  $\kappa' = 1$  (assuming a continuous aperture) for the lower bound, and  $S = S_u$ ,  $\kappa' = \kappa$  for the upper bound.

A direct consequence of our DoF bounds is that we expect the normalized singular values of the actual multipath channel to exhibit a heavy tail decay behavior beyond  $N = N_{0,l}$ , with singular value amplitude close to 1 for  $N \leq N_{0,l}$  and close to the reflectivities  $h(\mathbf{r}'_s)$  of the elements in  $S_u \setminus S_l$  for N > $N_{0,l}$ . In addition, due to our upper DoF bound, we expect the singular values to transition to 0 beyond  $N = N_{0,u}$ .

Note that for a *continuous*, closed aperture i.e.  $\Omega_{ap}=2\pi$ , we have  $S_u = S_l \cup S_i = S_l$  as  $m(S_l) = \Omega_{ap} = 2\pi$ . Therefore, in the  $\Omega_{ap}=2\pi$  case, we recover the results of [13] with no DoF increase beyond the LOS DoF i.e.  $N_l = N_u = 2W +$  $O(\ln{(2W)})$ . However, for all  $\Omega_{ap} < 2\pi$ ,  $N_{\epsilon}(\mathcal{E}_m) \geq N_l$ .

## V. NUMERICAL EXPERIMENTS

We now numerically evaluate the validity of Theorem 1 by considering the simulation setup shown in Figure 4. Our setup consists of a 1D SIMO aperture of length  $L_{ap}$  imaging a line target of length  $L_{ob}$  in the presence of two large planar reflectors of equal length  $L_{rf}$  centered at  $x = \pm D_{rf}, z =$  $-\frac{D}{2}$ . A single transmitter, indicated by the black triangle in Figure 3, illuminates the target with 30 GHz sinusoids, and the receive elements, indicated by circles in Figure 4, sample the backscattered data. The imaging target is located at a distance D along the z-axis from the aperture and makes an angle  $\theta$  from the x-axis. Throughout, we consider a 2D scattering model with the Green's function given by

$$\mathbf{G}(\mathbf{r}, \mathbf{r}') = \frac{j}{4} H_0^2 \left( k_0 \left| \mathbf{r} - \mathbf{r}' \right| \right), \tag{19}$$

where  $H_0^2(\cdot)$  is the 0-order Hankel function of the second kind. For the geometry under consideration,  $W=\frac{1}{2}k_0L_{ob}\cos\theta$   $\hat{\mathbf{G}}\left(s,\mathbf{r}'\right)$  respectively. Note that the normalized singular value and  $\Omega_{ap}=\frac{2L_{ap}}{\sqrt{L_{ap}^2+4D^2}}$ . Given the symmetry and the specular correspond to the Kolmogorov N-widths according to (15).

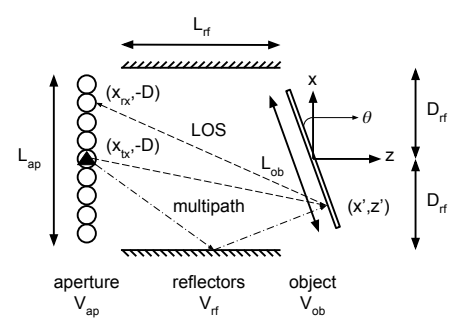


Fig. 4. System diagram for 2D SIMO imaging with specular reflectors.

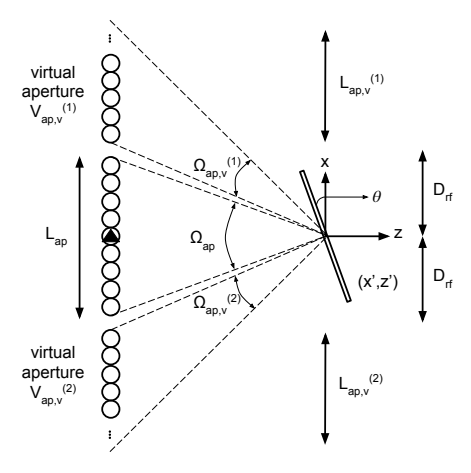


Fig. 5. Virtual aperture interpretation for Figure 4.

nature of the reflectors, we compute  $\Omega_{ap}^m$  by forming virtual apertures corresponding to both reflectors. In Figure 5 we show the virtual apertures for our setup. Thus,  $S_i$  consists of the azimuth angles of the rays joining the origin and points on the virtual apertures, and  $\Omega_{ap}^m = \Omega_{ap,v}^{(1)} \cup \Omega_{ap,v}^{(2)}$ . From Figure 3, it is clear that both reflectors induce virtual apertures of equal size  $L_{ap,v}^{(1)} = L_{ap,v}^{(2)} = L_{ap,v}$  such that  $\Omega_{ap}^m = 2\sin\theta_2 - 2\sin\theta_1$ , where  $\theta_2 = \tan^{-1}\left(\frac{2D_{rf} + \frac{L_{ap,v}}{2}}{D}\right)$ and  $\theta_1 = \tan^{-1}\left(\frac{2D_{rf} - \frac{L_{ap,v}}{2}}{D}\right)$ . Note that  $S_l \cap S_i = \emptyset$  here.

For simplicity, we let  $D_{rf} = \frac{L_{ap}}{2}$  and assume  $L_{rf}$  to be large enough such that  $L_{ap,v} = \min \left\{ L_{ap}, \frac{2D_{rf}}{D} L_{rf} \right\} = L_{ap}$ . From Theorem 1, we obtain

$$\frac{2L_{ap}L_{ob}\cos\theta}{\lambda\sqrt{L_{ap}^2 + 4D^2}} \le N_{\epsilon}\left(\mathcal{E}_m\right) \le \frac{6L_{ap}L_{ob}\cos\theta}{\lambda\sqrt{9L_{ap}^2 + 4D^2}},\tag{20}$$

where the terms with logarithmic dependence on  $N_{0,l}$  and  $N_{0,u}$  have been suppressed for clarity. Note that  $\kappa = 3$  here.

To numerically evaluate the DoF, we discretize (1) and observe the behavior of the normalized singular values of the LOS and combined multipath Green's functions  $G(s, \mathbf{r}')$  and  $\hat{\mathbf{G}}(s, \mathbf{r}')$  respectively. Note that the normalized singular values

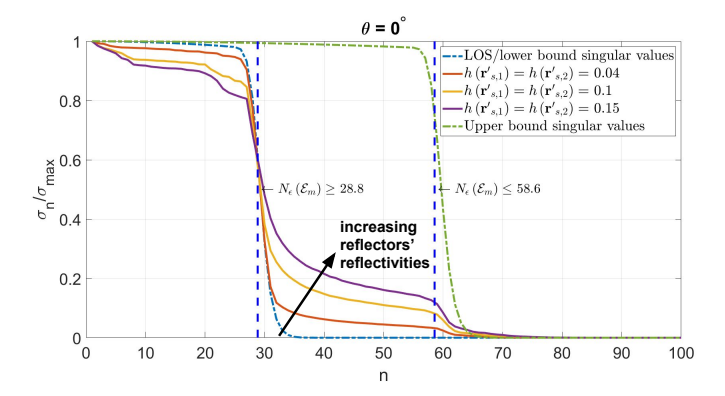


Fig. 6. Heavy tail decay behavior of multipath channel singular values with  $h(\mathbf{r}'_{s,1}) = h(\mathbf{r}'_{s,2}) = h$ .

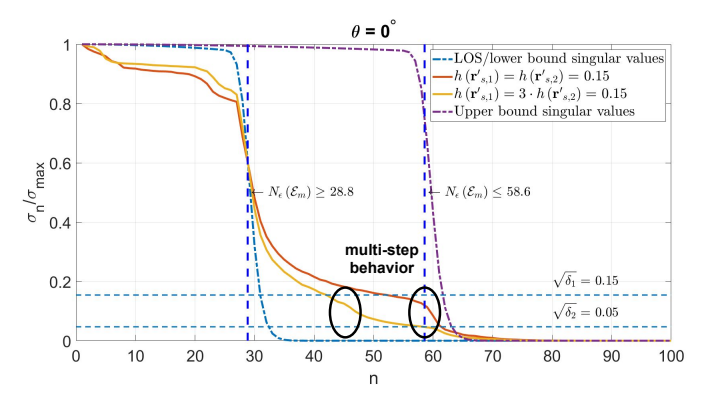


Fig. 7. Multi-step behavior of multipath channel singular values with  $h(\mathbf{r}'_{s,1})=3\times h(\mathbf{r}'_{s,2})=h.$ 

Throughout, we simulate our setup with the parameter values  $\lambda=1$  cm,  $L_{ap}=0.5$  m,  $L_{ob}=0.375$  m, D=0.6 m,  $D_{rf}=\frac{L_{ap}}{2},~L_{rf}=0.5625$  m. We simulate the interaction between the illuminating RF signals and all targets and reflectors via the Lambertian model presented in [21].

In Figure 6 we plot the normalized singular values for the LOS and multipath channels when both reflectors have the same reflectivity,  $h(\mathbf{r'}_{s,1}) = h(\mathbf{r'}_{s,2}) = h$ . We fix  $\theta = 0^{\circ}$ , and the reflectivity f of the target, and vary h. The upper and lower bounds in (20) evaluate to  $N_{0,l} = 28.8$  and  $N_{0,u} =$ 58.6 for the given values. The singular values corresponding to the choice  $S = S_l$  coincide with the LOS singular values; with multipath, the singular values exhibit a heavy tail decay with constant amplitude equalling h between  $N_{0,l}$  and  $N_{0,u}$ . We also plot the singular values corresponding to the choice  $S = S_u$ ; the DoF for this case is seen to match the number of non-zero multipath singular values. In Figure 7, we further illustrate the heavy tail decay behavior by constraining the reflectivity of one reflector to be  $3\times$  of the other reflector's reflectivity,  $h(\mathbf{r'}_{s,1}) = 3 \times h(\mathbf{r'}_{s,2}) = h$ . It can be seen that the singular values undergo a *multi-step* transition from h to  $\frac{h}{3}$  mid-way at  $\frac{N_{0,l}+N_{0,u}}{2}$  (due to the symmetry in the setup).

In Figure 8 we show the validity of our bounds across  $\theta$  by plotting  $N_{\epsilon}(\mathcal{E}_m)$  as a function of  $\theta$  for different values of  $\epsilon$ , 0.1460

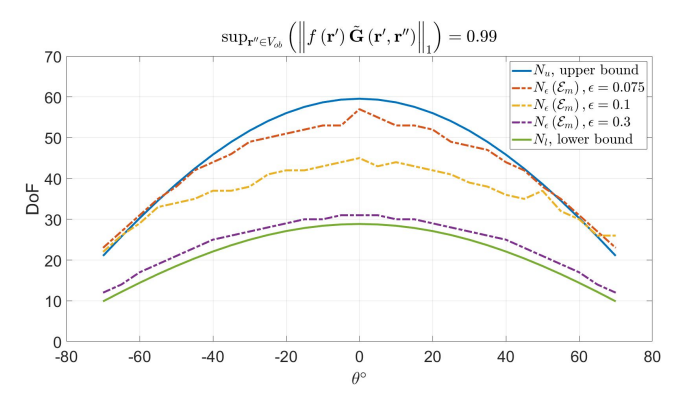


Fig. 8. Multipath DoF as a function of  $\theta$  for different values of  $\epsilon$ .

with the system parameter values chosen such that  $h(\mathbf{r'}_{s,1}) = h(\mathbf{r'}_{s,2}) = h$  and  $\sup_{\mathbf{r''} \in V_{ob}} \left( \left\| f(\mathbf{r'}) \, \tilde{\mathbf{G}} \, (\mathbf{r'}, \mathbf{r''}) \right\|_1 \right) = 0.99.$  As expected from the behavior of the singular values in Figure 6, we observe that  $N_{\epsilon} \, (\mathcal{E}_m)$  is well approximated by the upper bound for small  $\epsilon$  and by the lower bound for large  $\epsilon$ . For intermediate  $\epsilon$  values the curve lies between our predicted upper and lower bounds.

Our results clearly indicate an increase in the DoF with multipath; as the DoF is directly related to the imaging resolution, with larger DoF resulting in better resolution, this implies that super-resolution beyond conventional LOS imaging is a definite possibility for multipath-assisted imaging systems. The extent to which the additional DoF may be exploited, however, is highly dependent on the environment geometry and reflectivity in addition to the system precision;  $N_{\epsilon}\left(\mathcal{E}_{m}\right)$  is close to the upper bound only for small  $\epsilon$ .

#### VI. CONCLUDING REMARKS

In this paper, we presented a degrees of freedom analysis to quantify the amount of super-resolution possible with multipath-assisted imaging systems. Our analysis and main result indicate that the increase in DoF over LOS imaging is due to the interaction with the environment; thus, the environment geometry and reflectivity play a large role in determining the extent of super-resolution possible over LOS.

Our analysis indicates a heavy tail decay in the singular values between the lower bound (LOS DoF) and upper bound. Our main results remain consistent with [13] and predict no increase in the DoF when  $\Omega_{ap}=2\pi$  i.e. a continuous, closed aperture surrounding the imaging targets is used.

An important extension to our analysis would be the performance evaluation of multipath-assisted algorithms [6]–[11] to quantify the gap, if any, between the DoF upper bound and the actual performance of multipath-assisted algorithms.

We conclude by noting the close similarity between our results and the main results of [22], [23]. This is not surprising, given the common electromagnetic theory framework underlying both wireless communication and imaging [2], [3].

#### REFERENCES

- F. M. Dickey, L. A. Romero, J. M. DeLaurentis, and A. W. Doerry, "Super-resolution, degrees of freedom and synthetic aperture radar," *IEE Proceedings - Radar, Sonar and Navigation*, vol. 150, no. 6, pp. 419–429, Dec 2003.
- [2] M. Franceschetti, Wave Theory of Information. Cambridge University Press. Nov 2017.
- [3] D. A. B. Miller, "Waves, modes, communications, and optics: a tutorial," Adv. Opt. Photon., vol. 11, no. 3, pp. 679–825, Sep 2019.
- [4] O. Bucci and G. Franceschetti, "On the spatial bandwidth of scattered fields," *IEEE Transactions on Antennas and Propagation*, vol. 35, no. 12, pp. 1445–1455, December 1987.
- [5] O. M. Bucci and G. Franceschetti, "On the degrees of freedom of scattered fields," *IEEE Transactions on Antennas and Propagation*, vol. 37, no. 7, pp. 918–926, July 1989.
- [6] M. Cheney and R. J. Bonneau, "Imaging that exploits multipath scattering from point scatterers," in SPIE 5808, Algorithms for Synthetic Aperture Radar Imagery XII, E. G. Zelnio and F. D. Garber, Eds., vol. 5808. International Society for Optics and Photonics, May 2005, p. 142.
- [7] C. J. Nolan, M. Cheney, T. Dowling, and R. Gaburro, "Enhanced angular resolution from multiply scattered waves," *Inverse Problems*, vol. 22, no. 5, pp. 1817–1834, sep 2006.
- [8] V. Krishnan and B. Yazici, "Synthetic aperture radar imaging exploiting multiple scattering," *Inverse Problems*, vol. 27, no. 5, p. 055004, Mar 2011
- [9] M. Leigsnering, F. Ahmad, M. G. Amin, and A. M. Zoubir, "Compressive sensing based specular multipath exploitation for through-the-wall radar imaging," in 2013 IEEE International Conference on Acoustics, Speech and Signal Processing, May 2013, pp. 6004–6008.
- [10] R. Solimene, I. Catapano, G. Gennarelli, A. Cuccaro, A. Dell'Aversano, and F. Soldovieri, "Sar imaging algorithms and some unconventional applications: A unified mathematical overview," *IEEE Signal Processing Magazine*, vol. 31, no. 4, pp. 90–98, July 2014.
- [11] G. Gennarelli and F. Soldovieri, "A Linear Inverse Scattering Algorithm for Radar Imaging in Multipath Environments," *IEEE Geoscience and Remote Sensing Letters*, vol. 10, no. 5, pp. 1085–1089, Sep 2013.

- [12] R. Janaswamy, "On the em degrees of freedom in scattering environments," *IEEE Transactions on Antennas and Propagation*, vol. 59, no. 10, pp. 3872–3881, Oct 2011.
- [13] M. Franceschetti, M. D. Migliore, P. Minero, and F. Schettino, "The information carried by scattered waves: Near-field and nonasymptotic regimes," *IEEE Transactions on Antennas and Propagation*, vol. 63, no. 7, pp. 3144–3157, July 2015.
- [14] M. Franceschetti and K. Chakraborty, "Space-time duality in multiple antenna channels," *IEEE Transactions on Wireless Communications*, vol. 8, no. 4, pp. 1733–1743, 2009.
- [15] J. Xu and R. Janaswamy, "Electromagnetic degrees of freedom in 2-d scattering environments," *IEEE Transactions on Antennas and Propa*gation, vol. 54, no. 12, pp. 3882–3894, Dec 2006.
- [16] A. Pinkus, n-widths in Approximation Theory. Springer-Verlag, 1985.
- [17] M. Franceschetti, "On the information content of scattered waves," in 2012 IEEE International Symposium on Information Theory Proceedings, July 2012, pp. 1523–1527.
- [18] D. Slepian and H. O. Pollak, "Prolate spheroidal wave functions, fourier analysis and uncertainty — i," The Bell System Technical Journal, vol. 40, no. 1, pp. 43–63, Jan 1961.
- [19] H. J. Landau and H. O. Pollak, "Prolate spheroidal wave functions, fourier analysis and uncertainty — ii," *Bell System Technical Journal*, vol. 40, no. 1, pp. 65–84, 1961.
- [20] H. J. Landau and H. Widom, "Eigenvalue distribution of time and frequency limiting," *Journal of Mathematical Analysis and Applications*, vol. 77, no. 2, pp. 469 – 481, 1980.
- [21] M. Kotaru, G. Satat, R. Raskar, and S. Katti, "Light-Field for RF," Jan 2019. [Online]. Available: http://arxiv.org/abs/1901.03953
- [22] A. S. Y. Poon, R. W. Brodersen, and D. N. C. Tse, "Degrees of freedom in multiple-antenna channels: a signal space approach," *IEEE Transactions on Information Theory*, vol. 51, no. 2, pp. 523–536, Feb 2005
- [23] L. W. Hanlen, R. Timo, and R. Perera, "On dimensionality for sparse multipath," in 2006 Australian Communications Theory Workshop, 2006, pp. 125–129.